ELSEVIER

Journal of Hazardous Materials 76 (2000) 217–236

Journal of Hazardous Materials

www.elsevier.nl/locate/jhazmat

Phosphate immobilization using an acidic type F fly ash

Dennis G. Grubb *, María S. Guimaraes, Rodrigo Valencia

School of Civil & Environmental Engineering, Georgia Institute of Technology, Atlanta, GA 30332-0355, USA

Received 11 December 1999; received in revised form 24 February 2000; accepted 25 February 2000

Abstract

Batch equilibration experiments using a low calcium (~1 wt.% as CaO), acidic (pH ~4.5) Type F fly ash demonstrated phosphate immobilization on the order of 100% to 75% for 50 and 100 mg P/l solutions, respectively. A loosely compacted column of fly ash similarly removed 10 mg P/l for over 85 pore volumes. While the interactions between phosphate and calcium-rich (Type C) ashes are relatively well understood, insight into the mechanisms of phosphate immobilization in Type F ash necessitated a review of the phosphate chemistry and interactions with acidic geomedia. Phosphate adsorption was subsequently modeled using a constant capacitance model approach (CCM) excluding precipitation reactions. Our CCM predictions of total phosphate immobilization (20%) were substantially less than the results of the batch equilibration experiments and phosphate adsorption predicted by other researchers examining near pure natural and synthetic geomedia due to the compositional heterogeneity of the fly ash. Nevertheless, for the amorphous and crystalline phases studied, the immobilization of phosphate in the Type F fly ash is attributed to the formation of insoluble aluminum and iron phosphates at low to medium values of pH.

Keywords: Fly ash; Phosphate; Sorption; Precipitation; Acid conditions

1. Introduction

According to the American Coal Ash Association [1], sixty million tons of fly ash are produced annually in the United States, and only 25% to 30% of this material is productively re-used, principally in construction-related applications due to the pozzolanic characteristics of fly ash. The remaining 45 million tons are impounded or

* Corresponding author. Tel.: +1-404-894-7597; fax: +1-404-894-2281.
E-mail address: dgrubb@ce.gatech.edu (D.G. Grubb).

0304-3894/00/$ - see front matter
PII: S0304-3894(00)00200-4

landfilled. In seeking alternatives for productive reuse, coal burning and fly ash management activities are recognized to frequently occur in northern regions that also suffer from environmental problems due from phosphorous loading to surface and groundwater from concentrated agricultural activities including soil fertilization, feed lots, diaries, and pig and poultry farms. The National Water Quality Inventory 1994 Report to Congress cited nutrients (nitrogen and phosphorus) as one of the leading causes of water quality problems in rivers, lakes, and estuaries resulting in eutrophication, increased fish mortality and outbreaks of microbes such as *Pfiesteria piscicida*. Because fly ash is enriched with the oxides of aluminum, iron, calcium, and silica, fly ash emerges as candidate material to treat phosphate-laden effluents since aluminum, iron and calcium are known to strongly adsorb or precipitate phosphates in many agricultural, industrial and environmental applications [2,3]. To illustrate the general capabilities of fly ash to immobilize phosphate [4–11], we consider four studies.

Higgins et al. [10] explored the potential to treat eutrophic water (pH ~ 9) from Lake Charles East (IN) with total (suspended plus soluble orthophosphate) phosphorus concentrations of 600 μg P/l in a series of 1-liter jar tests using combinations of fly ash, lime and gypsum. Treatments with gypsum (100 to 500 mg/l) and fly ash (20 g/l) were found to be relatively ineffective in reducing the total concentrations of phosphate to below 60%, which increased with increasing gypsum dosage and with orthophosphate typically accounting for approximately 50% of the total phosphorus. A 90% reduction in orthophosphate was achieved with 500 mg/l gypsum dose when the pH was increased to 10. Lime, a stronger alkali, was subsequently used in conjunction with fly ash since its calcium content obviated the need for gypsum. Since a lime application of 300 mg/l to lake water (600 μg P/l; pH ~ 8.41) reduced the orthophosphate concentrations to 17 μg P/l with a final pH of 10.2, it was deemed that a lower lime dosage of 200 mg/l was a sufficient dosage rate given both the soluble phosphorus removal rate and lower final pH (41 μg P/l; pH ~ 9.4). While the addition of 20 g/l of fly ash had a small effect on the soluble concentrations, the primary benefit realized was significant reductions in the suspended phosphate concentrations, presumably due to the advantageous settling characteristics of fly ash solids. Using total lime and fly ash application rates of 200 mg/l and 20 g/l, respectively, a optimization study of material dosing and sequencing rates on lake water (640 μg P/l; pH ~ 8.9) showed that two sequential half dosages (100 mg/l, 10 g/l) achieved essentially the same phosphorus removal as the sequenced full dosages, but simultaneous application of the full dosages produced the overall lowest total phosphorus concentrations (150 μg P/l) without a substantial change in pH (~ 9.1). Algae studies performed in parallel with the jar test indicated that a 10 g/l dosage of fly ash was more effective than 300 mg/l of lime in reducing bacterial counts though it was not known whether the improvement resulted from more effective binding of phosphate and sealing of sediments after settling, removal of other growth factors, or the release of an inhibitory substance. An 85-day pond study using in-situ caissons as treatment cells showed dramatic reductions (> 95%) in soluble and total phosphorus concentrations when 20 g/l of fly ash and lime (500 mg/l) were added on Days 1 and 7, respectively.

In batch adsorption studies conducted at pHs of 5.25 and 8.25, Vordonis et al. [5] determined that the uptake of orthophosphate by four calcium-rich (10–32%) Greek fly

Table 1
Oxide Contents and PZC of high calcium fly ashes

Oxides Components						PZC	Reference
SiO_2	Al_2O_3	Fe_2O_3	CaO	MgO	SO_3		
45.3	26.2	7.6	10.1	6.5	1.9	9 ± 0.1	Vordonis et al. [5]
49.5	18.2	8.5	15	3.1	2.2	8.9 ± 0.1	
38.9	16.7	8.9	27.8	2.2	2.8	9.3 ± 0.2	
31.3	17.8	7.1	31.9	6.3	3.1	10.3 ± 0.1	

ashes exceeded the amount predicted by monolayer coverage, which suggested either multilayer adsorption or precipitation (see Table 1). The fly ashes also contained magnesium at 2.2% to 6.3% and had specific surface areas (SSA) of 5.1 to 6.7 m^2/g. To distinguish between these two mechanisms of immobilization, several additional properties were determined: the zero points of charge (ZPC) varied between 8.9 and 10.3 (pH) units, and the isoelectric points (IEPs) were on the order of 7.0 to 8 units. The oxide chemistry of the ashes (see Table 2) and their large positive surface charges (i.e., below their ZPCs) suggested that the electrostatic binding of anions would be the preferential mechanism of phosphate uptake. Ash samples prewashed with potassium nitrate (0.01 mol KNO_3/dm^3) at pH 5.25 showed no difference in phosphate uptake except for a sample containing 31.9% calcium that underwent a large decrease in phosphate uptake. It was thought that calcium phosphate may have formed in the unwashed sample but no calcium phosphate was detected by X-ray fluorescence (XRF). Given the chemically heterogeneous nature of fly ash, the presence of magnesium also suggested that the formation of apatite precipitates would be inhibited [12]. In the ashes exposed to phosphate solutions, adsorbed phosphate bands (PO_4^{3-}) were detected by IR spectroscopy, but the acidic phosphates ($H_2PO_4^-$, HPO_4^{2-}), which are mostly soluble in the pH range of 5 to 9 [13] were not detected. A shift in the IEPs of the ashes to a more acidic condition suggested that phosphate sorption occurred as opposed to the formation of apatite, which would have resulted in a more basic IEP.

Ugurlu and Salman [6] conducted batch and columns experiments with a calcium-rich (34%) fly ash with a LOI of 10% and an average particle size between 0.125 and 0.063 mm. Adsorption studies were conducted with 20, 50 and 100 mg P/l solutions at constant pH (not reported) at temperatures between 27°C and 50°C. Adsorbent doses of fly ash from 4 to 20 g/l produced over 95% removal of phosphate (20 mg P/l) for

Table 2
PZC of selected minerals

Minerals	PZC	Reference
Hematite	8.5	Breeuswama and Lyklema [44]
Mullite	5.6	
$\alpha - Al_2O_3$	9.1	Sposito [42]
SiO_2	2.9	

contact times as little as 5 min. When the phosphate concentrations were increased to 50 and 100 mg P/l at the lowest adsorbent dose (4 g/l), phosphate removal by fly ash was still greater than 93% and 60% for contact times greater than 10 min, respectively, with peak adsorption observed at 40°C. However, the role of pH (initial stock solution, or equilibrated solution) was not discussed. In a 5-cm diameter, 65-cm long column packed with fly ash permeated with the 100 mg P/l solution with a residence time on the order of 60 min, the phosphate removal efficiency and effluent pH respectively decreased from 95% to 80% and 11.29 to 8.83 pH units over a 72-h period. When the fly ash from the bottom (outlet) of the column was exhumed and analyzed by XRF, it was very similar to the unused ash except that a significant reduction in calcium content was observed (8%), suggesting that calcium dissolution occurred within the entire column and that the mobilized calcium was purportedly available to precipitate the dissolved phosphate. Additional batch studies conducted at high pH (>11.5) confirmed calcium dissolution from the fly ash. X-ray diffraction (XRD) analyses of the fly ash exhumed from the column confirmed the appearance of amorphous apatite at the inlet, which became more crystalline with time. Phosphate sorption was implied by the XRD response that showed decreased masking of calcite surfaces along the longitudinal axis of the column. It was therefore concluded that adsorption of phosphate to calcite surfaces was the dominant immobilization mechanism.

The Electrical Power Research Institute (EPRI) [9] describes the land application of 345.22 metric tons/ha of an acidic coal ash containing 1.75 kg/ha of phosphorous to existing soils. Land application is a frequent fly ash disposal option accounting for 7.5% of the total amount of fly ash reuse, where the predominant application is for mine reclamation [1]. After the land application the bio-available phosphorous content in the fly ash–soil mixture was measured to be 33.63 kg/ha, substantially less than the 56.04 kg/ha measured in the soil before the land application. While the fly ash initially contained phosphorus, it was still capable of immobilizing an additional 22.42 kg/ha.

The reviewed articles and their citations suggested that the literature dealing with phosphorus and fly ash is dominated by calcium-rich ashes (Type C) not Type F ashes. The mechanism of phosphate immobilization in Type C ash was linked mainly to the formation of calcium phosphate, namely hydroxyapatite, at elevated pH. However, these studies remain somewhat relevant to Type F ashes because calcium often leaches from ash and the pH drifts with continued leaching or chemical weathering in aggressive environments. It appears that phosphate immobilization in acidic Type F ashes has not been extensively researched and the mechanisms of phosphate immobilization are expected to be very different based on mineralogical differences. To illustrate these differences, we provide an overview of the relevant phosphate chemistry, fly ash mineralogy and phosphate interactions with calcium deficient porous media that is then integrated with the results of our batch experiments and numerical modeling efforts.

2. The chemistry of phosphate immobilization

The most frequently encountered species of phosphates in natural waters and effluents are orthophosphates ($-PO_4$), pyrophosphates ($-P_2O_7$) and tripolyphosphates

($-P_3O_{10}$) [13]. Orthophosphates are regulated by pH since phosphoric acid is triprotic with acidity constants of $10^{-2.1}$, $10^{-7.2}$ and $10^{-12.3}$ for the successive deprotonation reactions, as shown in Fig. 1. Consequently, the acidic phosphates ($H_2PO_4^-$, HPO_4^{2-}) are the predominant aqueous species for the pH range of 5 to 9 [13]. Polyphosphates ($H_2P_3O_{10}^{3-}$, $HP_3O_{10}^{4-}$, $HP_2O_7^{3-}$) may also be present in the same pH range but typically at concentrations less than the orthophosphates [14]. Phosphate immobilization has been extensively researched in two main fields, wastewater treatment [14–20] to prevent eutrophication of receiving (surface) waters, and soil science to understand the fate of the phosphate present in fertilizers [7,21–33].

In wastewater applications, the most common and successful methods to precipitate phosphate involve the dissolved cations Al^{3+}, Ca^{2+}, Fe^{3+} and to a lesser extent Fe^{2+} [14]. Iron and aluminum are typically administered as chloride (Fe) or sulfate salts (Fe, Al) whereas calcium is added as a lime (CaO). Solubility diagrams for metal phosphates in pure water show that when iron and aluminum are present, strengite ($FePO_4$) and variscite ($AlPO_4$) are the stable solid phases in the low pH range (< 6.5). The minimum variscite solubility occurs at pH 6, i.e., 1 pH unit higher than strengite. At higher pHs (> 6.5), the iron and aluminum chemistry becomes increasingly governed by the formation of oxides and hydroxides, and these conditions are more ideal for the precipitation of phosphate with calcium as apatites and hydroxyapatites even though the solubility of calcium is regulated by calcite ($CaCO_3$). In wastewater at neutral to mildly alkaline conditions, magnesium also promotes the formation of beta-tricalcium phosphates (β-$Ca_3(PO_4)_2$) and struvite ($MgNH_4PO_4$) if ammonia is also present, and

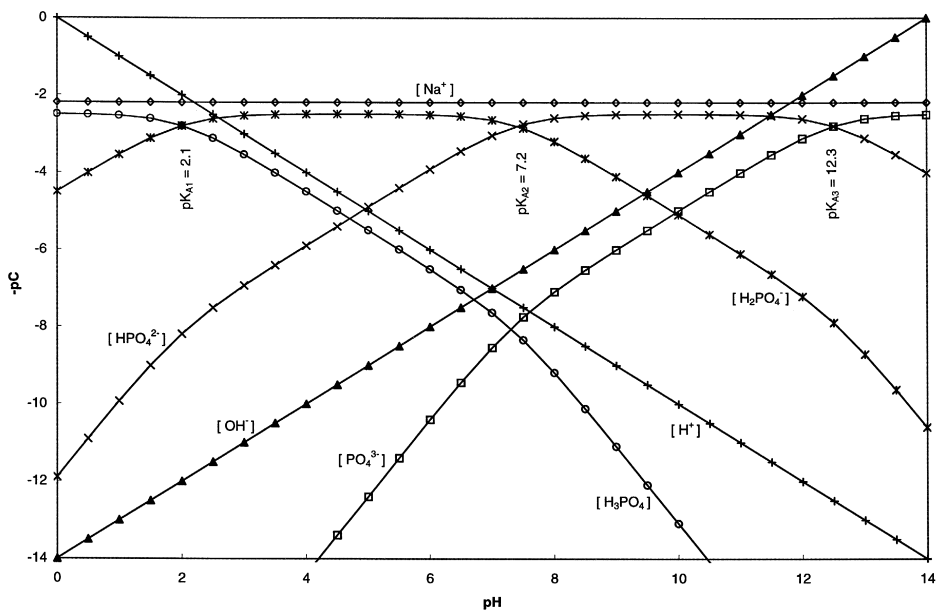

Fig. 1. pC–pH diagram for a 3.22×10^{-3} M Na_2HPO_4 solution.

calcium itself may be scavenged and incorporated into magnesium calcium carbonates if enough carbon is present [14].

Soil science research has focused on the optimal range of pH for phosphorus to remain in solution and thus bio-available. The fate of phosphorus appears to be more related to adsorption process on mineral or particle surfaces rather than precipitation, which is the chief approach of water treatment. For most crops, the optimum pH in terms of nutrients availability ranges between 6 and 6.8, which corresponds to phosphorus occurring as dissolved HPO_4^{2-} and $H_2PO_4^-$. Phosphorus is generally considered insoluble at extreme pHs, i.e., below 5.5 and above 7.5. Phosphate adsorption onto mineral surfaces is most often regulated by the electrostatic attractions of the soluble phosphate ions and mineral surface. Phosphate ions are negatively charged, and are therefore attracted to the positively charged sites that are common to acidic soils. Phosphorous is strongly complexed with the constituents of acidic soils, namely iron and aluminum [24,34,35]. These soils are also typically deficient in calcium, as are type F ashes, and the relevance of iron and aluminum based interactions will be discussed later.

3. Fly ash mineralogy

Coals are composed of aluminosilicates (clays), carbonates, sulfides, chlorides and quartz that are oxidized at high temperatures (above 1500°C), which melts almost all of the inorganic components with the exception of quartz. The resulting fly ash typically has spheroid morphology with particle sizes ranging from less than a micron to several microns [36]. The ash particles evaluated by Dudas and Warren [36] were found to be predominately comprised of solid spheres, plerospheres (hollow spheres containing smaller spherical particles) and cenospheres (empty hollow spheres). They proposed a structural model for fly ash to aid in leaching experiments depending on the solid or hollow nature of the spheres. Solid particles were characterized by an exterior hull composed of aluminosilicate glass with embedded or accreted inorganic salts and oxides that are more reactive than the interior glass matrix. A thin shell of mullite ($Al_6Si_2O_{13}$) also may be located at or near the surface of the particle. However, mullite was found to be more closely associated with the surface of hollow spheres lacking a hull and featuring surface accretions of inorganic salts and oxides. Dudas and Warren [36] suggested that the exterior hull and the associated surface salts and oxides on the fly ash particles determine the sorption, leaching and weathering behavior of the ash.

Fast and slow rates of cooling result in the formation of amorphous and crystalline phases, respectively. The percentage of amorphous versus crystalline phases in fly ash varies considerably depending on the burning process. McCarthy et al. [37] surveyed 178 samples of fly ash from North America and observed that the crystalline portion of the fly ashes typically accounts for 20–40% of the ash. XRD patterns of fly ash indicate the presence of mullite ($Al_6Si_2O_{13}$), magnetite (Fe_3O_4), hematite (α-Fe_2O_3), spinel ($MgAl_2O_4$) and quartz (SiO_2) [37,38]. The occurrence of these constituents depends on the cooling process. McCarthy [39] shows XRD patterns of different fractions of fly ash with a notorious increase in the amorphous phase in the smaller fractions. The amorphous phase is composed primarily of aluminosilicates and the oxides of aluminum,

Table 3
Chemical composition of various fly ashes in terms of the oxide contents

Material	Source	Sample size size	Composition (wt.%)									Reference
			SiO_2	Al_2O_3	Fe_2O_3	CaO	MgO	K_2O	Na_2O	P_2O_5	MnO	
Low calcium fly ash (< 10% CaO)	USA	45	52.5	22.8	7.5	4.9	1.3	1.3	1.0	N/R	N/R	McCarthy et al. [37]
	Pennsylvania	1	51.8	28.2	14.3	1.0	0.5	2.1	0.1	0.3	0.06	This study
Intermediate calcium fly ash (10–19.9% CaO)	USA	36	48.5	19.6	6.2	15.2	3.2	0.8	1.5	N/R	N/R	McCarthy et al. [37]
High calcium fly ash (> 20% CaO)	USA	97	36.9	17.6	6.2	25.2	5.1	0.6	1.7	N/R	N/R	McCarthy et al. [37]

N/R: Not reported.

calcium, iron, magnesium, sodium and potassium. The amorphous phase appears in XRD patterns as a broad halo centered approximately between 22° and 35° $2\theta_{max}$, under the principal line of mullite [38]. The distribution of the minerals of the crystal phases depends on the type of coal burned. Mullite is found in bituminous and subbituminous ashes and it is usually absent from lignite ashes [36,38]. Hematite and spinel are found in considerable quantities in bituminous ashes, but are absent from low rank fly ashes; and quartz can be found in different proportions in all types of ashes.

The chemical composition of various fly ashes in terms of the oxide components is presented in Table 3. Fly ashes derived from lignite coal are more likely to have high calcium contents. De Groot et al. [40] surveyed 50 different coal fly ashes and found that the pH of solutions containing fly ash varied from 4 to 12.5 depending on the major element composition. This trend was also confirmed on the basis of five fly ashes by Theis and Wirth [8] who demonstrated that the maximum pH shift was attained with fly ash dosages as low as 1–2 mg/l. The pH shifts where found to be most closely correlated with the oxalate extractable iron (Fe_{ox}) and soluble calcium content at pH 3 ($Ca_{pH=3}$). Calcium deficient ($Fe_{ox}/Ca_{pH=3} > 3$) fly ashes were associated with equilibrated pHs between 3 and 5 for the fly ash dosages of 200 g/l.

4. Montour ash characteristics

The subbituminous fly ash used in this study was obtained from electrostatic precipitator bins of the Pennsylvania Power & Light (PP&L) Montour facility located in Washingtonville, PA. A particle size analysis of the fly ash revealed that the ash is fairly uniform and composed of clay-sized particles with a mean diameter (d_{50}) of 0.02 mm according to ASTM-422. Fig. 1 shows a random sample of spherical fly ash particles with particle diameters ranging between 0.001 mm (1.7 μm) and 0.02 mm (20 μm), as determined using a scanning electron microscope (Hatachi S4100) with an integrated with a Noran light element energy dispersive X-ray spectrometer (SEM/EDX). Fig. 1 shows a typical feature of fly ashes that is plenospheres filled with smaller diameter spheres. The specific surface area of a random ash sample was determined to be 1.3 m^2/g based on a single point BET isotherm test completed by Micromeretics (Norcross, GA).

X-ray Fluorescence (XRF) was used to determine the chemical composition of the fly ash by Resource Materials Testing (Clermont, GA). The results of the XRF analyses suggest that the elemental chemistry is dominated by silica, aluminum and iron, as summarized in Table 3. The low calcium content (~ 1 wt.%) and the low carbon content (1.7 wt.%) determined by the loss on ignition (LOI) test suggests that precipitation and adsorption processes will be controlled by the interactions with reactive silica, aluminum and iron sites and not interactions involving calcium or magnesium oxides. XRD analyses of the Montour ash were completed using a Rigaku DMAX-B diffractometer (Cu radiation source) linked to powder diffraction database JCPDS that indicated that mullite, quartz and hematite were the key crystalline phases. One of the striking features of this ash is that while a Class F ash is defined as having no less than 70 wt.% SiO_2, Al_2O_3 and Fe_2O_3 (combined) by ASTM C618, these oxides sum to 94% for the

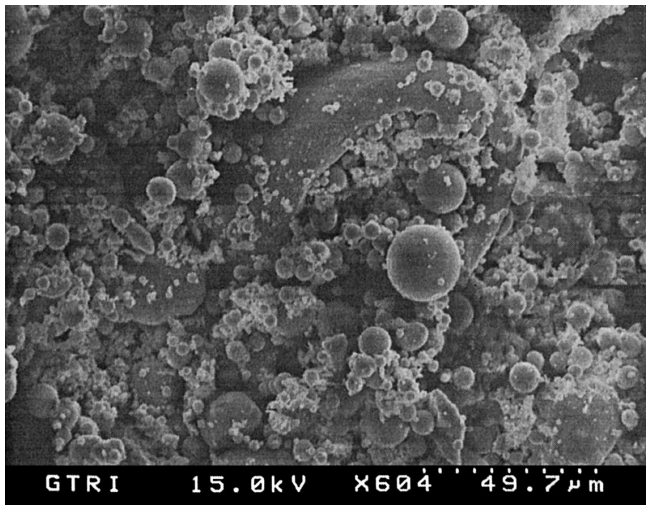

Fig. 2. SEM micrograph of Montour fly ash.

Montour ash. Modified toxicity characteristic leaching procedure (TCLP) tests indicated that there are essentially no leachable heavy metals from the Montour ash (Fig. 2).

5. Phosphate immobilization experiments

Batch equilibration experiments were conducted using the Montour ash and phosphate stock solutions containing 50, 75 and 100 mg P/l. Glass equilibration vials were presoaked in a 3% nitric acid bath for no less than 24 h and were sequentially rinsed with a 3% nitric acid solution and B* Pure water prior to use. B* Pure water purified by organics and metals removal cartridges having a specific resistance of 17.8 MΩ cm was used to prepare the phosphorus stock solutions. Phosphorus was added as dibasic anhydrous sodium phosphate (Na_2HPO_4, 99.6% purity) to the B* Pure water (pH = 5.5) to produce the stock solutions. The initial pHs of the stock solutions were 8.60, 8.62 and 8.56, for the 50, 75, and 100 mg P/l solutions, respectively. The increase in the pH of the deionized water after addition of Na_2HPO_4 is attributed to the formation of $H_2PO_4^-$ ions, which scavenge protons (H^+) from the bulk solution thereby increasing pH, as suggested by Fig. 1 for a 100 mg P/l solution (3.22×10^{-3} M Na_2HPO_4).

Deionized water blended with fly ash at a ratio of 10:1 (wt.%) produced an equilibrated leachate pH of approximately 4. An equilibrated leachate pH of 4.25 was obtained when fly ash was added to tap water (pH = 6.64) indicating that the equilibrated acidity of the leachate is relatively independent of the initial water source (deionized vs. tap water). For the batch phosphate immobilization experiments, the stock solutions were added to glass vials containing premeasured quantities of fly ash to achieve a liquids:solids ratio of 10:1. Triplicate samples were equilibrated on an orbital shaker (100 RPM) and the solution pH, and phosphate and sulfate concentrations were

determined at select intervals up to 96 h. Leachate samples were collected using latex free syringes fitted with styrene based strong acid resin syringe filters (OnGuard-H). Aqueous phosphate and sulfate concentrations were analyzed using a Dionex DX-500 high performance ion chromatograph (IC) fitted with an ED40 electrochemical detector having a background conductivity between 2 and 3.5 μS. Ion separation was accomplished using a 25 ul sample injection loop on an Ionpac AS16-4 mm column using a 35 mM NaOH eluent at a flow rate of 1.5 ml/min.

The equilibrated pH, and phosphorus and sulfate concentrations for 10:1 solution:fly ash mixtures versus initial phosphorus concentration and time are shown in Figs. 3–5, respectively. Fig. 3 illustrates that significant pH changes occur when the stock solution is added to the Montour ash, as indicated by the difference between the initial pH of stock solution (pH_0) and the equilibrated values (pH ~ 4–6). Fifty milligrams per liter of phosphorus had virtually no effect on the solution pH in the presence of fly ash. Fig. 4 demonstrates phosphate immobilization on the order of 100% to 75% for 50 and 100 mg P/l solutions, respectively. The removal of phosphate by the Type F ash used our experiments is comparable or greater than that by the reviewed applications using Type C ash [5,6,10]. Fig. 5 shows that the fly ash released approximately 1230 mg SO_4^{2-}/l into solution and that this concentration was essentially unaffected by the presence of phosphate in the deionized water.

A column experiment was also conducted using a 7-cm diameter, 14-cm long sample of pure Montour ash compacted to a loose condition by moist tamping. A 10 mg/l phosphate stock solution was prepared as described above. A reservoir of the stock

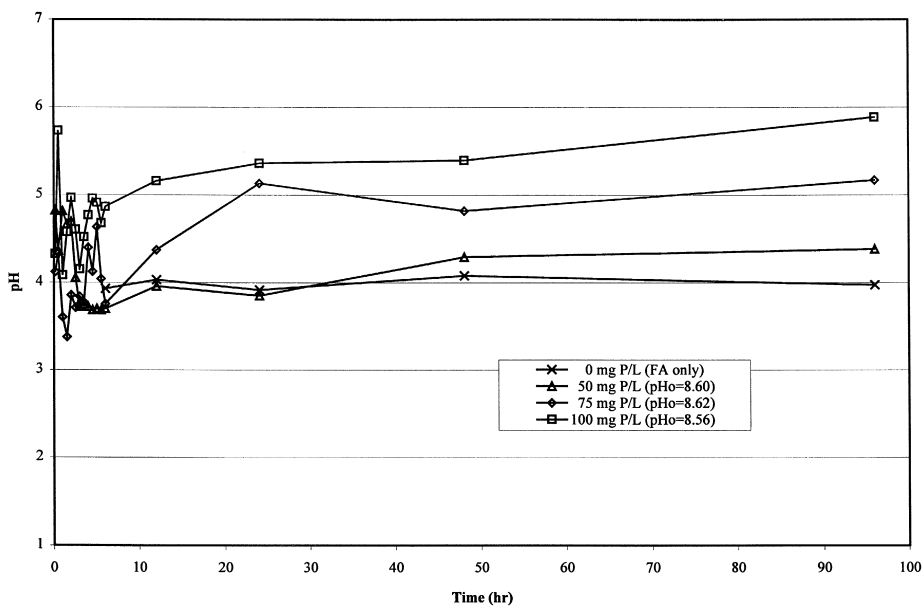

Fig. 3. Equilibrated pH for 10:1 solution:fly ash batch mixtures versus initial phosphorus concentration and time.

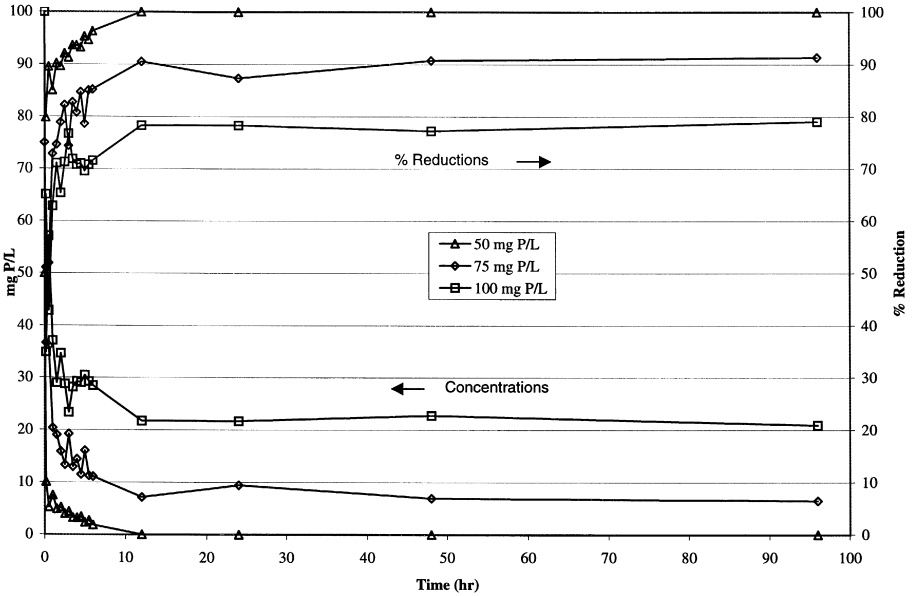

Fig. 4. Equilibrated phosphorus concentrations for 10:1 solution:fly ash batch mixtures versus initial phosphorus concentration and time.

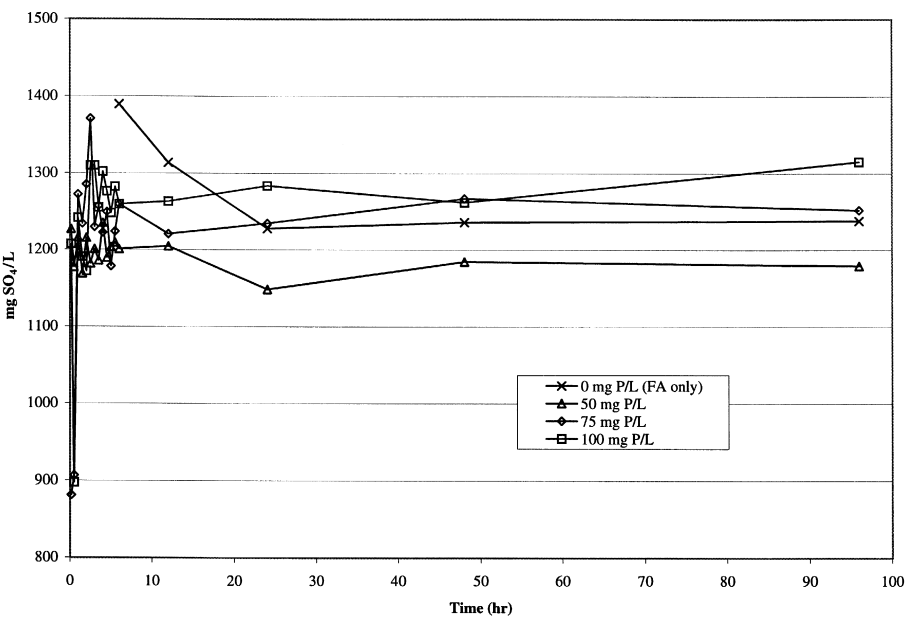

Fig. 5. Equilibrated sulfate concentrations for 10:1 solution:fly ash batch mixtures versus initial phosphorus concentration and time.

solution had an initial pH of 8.5. Influent and effluent samples were collected at locations immediately upgradient and downgradient of the column and it was determined that the column of pure Type F ash immobilized phosphate at dissolved concentrations of 10 mg P/l for over 85 pore volumes.

6. Interactions between phosphate and calcium-deficient media

In order to evaluate which mineral phases and interactions are responsible for phosphate immobilization in the batch experiments, it is important to recall that the metal oxide chemistry of the fly ash does not distinguish between the occurrence of the elements in an amorphous or crystalline phase, or the actual mineral or compound. The most dominant elements reported for Type F ashes are silicon, aluminum, and iron, as suggested by Table 3. Even though the silica content of the Montour ash is high, and quartz appears in most ashes, the low point of zero charge of quartz (PZC ~ 1.8–2.9) [41,42] enables it to retain a net negative surface charge for the normal range of pH encountered for most natural waters [43]. Therefore, quartz is not expected to adsorb significant quantities of phosphorus. Consequently, in calcium and magnesium deficient media, the principal reactions with phosphate are likely to involve iron and aluminum-based minerals, depending on the pH of the system. The principal crystalline iron and aluminum compounds in low calcium ($< 10\%$) Type F ashes are hematite and spinel, and mullite, respectively [39], but spinel was not detected by XRD for the Montour ash. The principal form of amorphous aluminum is amorphous aluminosilicate. To provide insight to the relevant interactions for the aluminum and iron compounds, it will be helpful to consider soil science research since it has focused on phosphate interactions with natural and synthetic iron- and aluminum-rich minerals, media and soils and has demonstrated that phosphorus binds strongly with the iron and aluminum constituents in acidic soils [22,24,27,31–35].

Hematite has a PZC on the order of 8.5 to 9.1 [41,44]. Below the PZC, hematite is characterized by protonated surface hydroxyl (SOH_2^+) groups that have the ability to form inner sphere complexes with the phosphate ions that become so strongly attached that sorption is essentially independent of the solution ionic strength [24,42,43]. Hematite, however, has limited sorption capacity for anions compared to other iron bearing minerals and oxides due to its crystallinity. For example, the reactive surface sites present in the basal planes of hematite are not able to adsorb phosphate [20,30,31,33]. Baker et al. [20] researched phosphate removal by different iron and aluminum oxides. They found that the rate of phosphate removal was much less using iron oxides than using steel foundry oxides.

Aluminum is present in fly ash either as amorphous aluminosilicates or mullite. Although mullite will not uptake as much phosphate as hematite, it must be included as an important potential sorbent since it is generally present in relatively high amounts and often covers fly ash particles with a thin shell [36]. Mullite has not been as extensively researched as other aluminum bearing minerals because of its complexity. However, some insight on mullite can be gained by considering the interaction of phosphate with other aluminosilicates such as kaolinite [45]. van der Hoek et al. [45] indicated that both

minerals have AlO and SiO surface groups that are likely to behave similarly. The difference in the structure and charge distribution between kaolinite and mullite will affect the sorption affinity, and thus, the results from kaolinite can only be qualitatively compared to mullite. The interaction between phosphate and either one of the amorphous phases of fly ash (amorphous iron and amorphous aluminosilicate) is expected to result in considerable phosphate immobilization. Higher adsorption is expected in these phases as compared to the crystalline phases, the main reason being that the disorganized internal structure of amorphous materials is associated with greater reactivity and site densities.

Phosphate adsorption by acidic soils and synthetic aluminosilicates was researched by Veith and Sposito [46], who observed that phosphate interactions with aluminosilicates were characterized by: (1) slow approach to equilibrium, (2) dissolution of silica from mineral structure, and (3) formation of Al–P compounds involving high quantities of P (almost 82% of P that was added to aluminum on an equimolar basis) though the nature of the formed phase is not accurately known. The influence of the silica/aluminum ratio on phosphate sorption was studied by Yuan [47] for three synthetic amorphous aluminosilicates and three soil samples. The sample with lowest Si/Al ratio, i.e., the highest aluminum content, retained the largest amount of phosphorous. Among aluminum bearing materials, noncrystalline hydrous aluminum oxides have higher bonding energy with phosphates than aluminum silicates and crystalline sesquioxides [46,47]. Additionally, the mechanism of phosphorous sorption on mineral surfaces is believed to be adsorption followed by precipitation [29,30]. This observation was supported by the appearance of crystalline phases after approximately 18 days of testing [30]. However, it was argued whether early precipitation could have been interpreted as adsorption due to the lack of techniques able to identify the formation of very small crystals [30].

7. Modeling phosphate interactions with type F fly ash

The adsorption of phosphate by fly ash has been represented with empirical relationships such as Fruendlich and Langmuir sorption isotherms (see Ref. [6] for detailed references). However, these isotherms are simply fitting curves and lack the sophistication to account for pH dependent behavior and the multiple valence states of dissolved phosphate species [25]. The batch experiments underwent large pH shifts, which changes the dominant phosphate species in the solution ($H_2PO_4^-$ or HPO_4^{2-}) as suggested by Fig. 1. It is therefore more appropriate to model such systems using approaches other than with Langmuir or Freundlich sorption isotherms.

Modeling the interactions of phosphate with the solid phase typically utilize surface complexation models (SCMs), which simulate the adsorption reactions occurring at the (crystal) mineral–water interface. For example, the computer program HYDRAQL evaluates chemical equilibria in aqueous batch systems and ion adsorption onto oxide minerals using SCMs [48]. Different SCM models are available that represent different mineral–water systems, i.e.: (i) constant capacitance model (CCM); (ii) diffuse layer model (DLM); (iii) triple-layer model (TLM); and (iv) four-layer model. The selection

Table 4
Typical values of site density for selected minerals

Minerals	Site density (sites/nm^2)	Reference
Hematite	10	Davies and Kent [43]
Mullite	0.55	He et al. [51]
Amorphous iron	6.7	Goldberg and Sposito [24,25]
Amorphous aluminum	2.6	Goldberg and Sposito [24,25]

of the model to represent the mineral–water interface is governed by the binding mechanism between solute and solid and its dependence on the solution ionic strength. The CCM approach was selected because it assumes hydrogen, hydroxyl and inner sphere complexing ions (such as phosphate) are adsorbed in the same plane without ionic strength influencing the adsorption process. The CCM also requires less number of constants than other models. More importantly, phosphorous adsorption on hematite, corundum, and goethite has been successfully modeled using a CCM approach by Goldberg et al. [24–26,28]. Selenite and arsenate adsorption on the mullite phase in fly ash was also modeled with a CCM by van der Hoek et al. [45], who determined that selenite and arsenate form inner-sphere complexes with aluminum and iron, and that the reaction rate of selenite and arsenate is very rapid with the maximum arsenate sorption occurring within 2 h. The sorption of arsenate and selenite also has been successfully modeled on kaolinite by Goldberg and Glaubig [49,50]. Modeling phosphate–mullite interactions with CCM is therefore considered to be valid for phosphate based on the aforementioned considerations. Lastly, phosphate adsorption on γ-Al_2O_3 and kaolinite was modeled with a CCM to evaluate the competing mechanisms between phosphates and sulfates [51]. He et al. [51] showed a competing sorption mechanism between SO_4 and PO_4 and suggested that SO_4 does not compete effectively with PO_4 for adsorption sites, because SO_4 appears to form outer-sphere complexes. Phosphate adsorption on amorphous synthetic aluminum and iron phases also has been successfully modeled with CCM [24]. However, while phosphate and sulfate have been modeled and inner and

Table 5
Equations modeled by constant capacitance model

Reaction	Equilibrium constants
$FeOH + H^+ \rightarrow FeOH^+$	K_+^{Fe}
$FeOH - H^+ \rightarrow FeO^-$	K_-^{Fe}
$AlOH + H^+ \rightarrow AlOH^+$	K_+^{Al}
$AlOH - H^+ \rightarrow AlO^-$	K_-^{Al}
$FeOH + PO_4^{3-} + 3H^+ \rightarrow FeH_2PO_4 + H_2O$	K_1^{Fe}
$FeOH + PO_4^{3-} + 2H^+ \rightarrow FeHPO_4^- + H_2O$	K_2^{Fe}
$FeOH + PO_4^{3-} + H^+ \rightarrow FePO_4^= + H_2O$	K_3^{Fe}
$AlOH + PO_4^{3-} + 3H^+ \rightarrow AlH_2PO_4 + H_2O$	K_1^{Al}
$AlOH + PO_4^{3-} + 2H^+ \rightarrow AlHPO_4^- + H_2O$	K_2^{Al}
$AlOH + PO_4^{3-} + H^+ \rightarrow AlPO_4^= + H_2O$	K_3^{Al}

Table 6
Representative surface complexation constants for minerals occuring in Type F ash

Mineral	log K_1	log K_2	log K_3	Reference
Kaolinite	N/A	22.37	17.14	He et al. [51]
α-Fe_2O_3	7.43	2.06	−4.23	Breeuswama and Lyklema [44]
Amorphous iron	33.54	27.3	21.05	Anderson and Malotky [53]
Amorphous aluminum	29.49	23.89	N/A	Rajan et al. [54]

N/A = not available.

outer sphere complexes, respectively [51], Fig. 5 suggests that there may not be competitive adsorption effects between phosphate and sulfate, given the quantity of sulfate released by the fly ash. Since both anions desorb with increasing pH, the pH data for the 100 mg P/l curve at 96 h (1.5 pH units greater than for 0 and 50 mg P/l equilibrated solutions) may suggest that additional sulfate is being released by the fly ash rather than it being displaced from the fly ash surface by phosphate.

A capacitance constant of 1.06 F/m^2 was used and the ionic strength of the solution was chosen to be 0.1 M though it is not anticipated to influence the interactions between phosphate and iron and aluminum compounds [43]. It was assumed that each of the mineral phases acted independently. Sorption of phosphate was modeled on the basis of the crystalline minerals reported by XRD, i.e., hematite and mullite; and amorphous iron and aluminum. Due to the lack of quantitative data reported on XRD for the Montour ash, the percentage distribution of each phase was calculated based on average values given by McCarthy [39]: 3.9% hematite, 10.4% mullite, 17.81% amorphous aluminum, and 10.43% amorphous iron. The total surface area was that determined using the BET isotherm: 1.3 m^2/g. A surface site density of hematite 10 sites/nm^2 was assumed based on the acid-base titration method [25]. Due to the lack of phosphate binding constants for mullite, phosphate–mullite interactions were modeled on the basis of kaolinite following the approach of van der Hoek et al. [45]. The site density values adopted for the amorphous phases are presented in Table 4. The reactions presented in Table 5 were used to model sorption and the corresponding average surface complexation constants are summarized in Tables 6 and 7, which should be taken to *qualitatively* describe phosphate adsorption since even in synthetic oxides surfaces multiple types of surface sites are capable of adsorbing phosphates [43,51]. For illustrative purposes, the CCM simulation assumed an initial phosphorus concentration of 50 mg P/l, which was completely immobilized by fly ash, see Fig. 1.

Table 7
Representative surface protonation constants for minerals occuring in Type F ash

Surface Group	K_+	K_-	Reference
FeOH	8.05	−8.95	Breeuswama and Lyklema [44]
AlOH	7.89	−9.05	Huang and Stumm [55]

8. Results and discussion

Fig. 6 presents the results of the SCM for pH ranging from 4 to 10 using the CCM approach for an initial phosphorus concentration of 50 mg P/l. The adsorption of phosphate onto amorphous iron oxide increased with decreasing pH and essentially stabilized at 12% below pH 7. A somewhat similar trend was observed with amorphous aluminum in that the immobilized phosphate varies between 4% and 6% below pH 8. The adsorption of phosphate on hematite decreased from 4% with increasing pH due to the surface sites of hematite becoming more negatively charged toward its point of zero charge (8.5). Phosphate adsorption on kaolinite, although negligible compared to that of hematite, was consistent with the trends reported by He et al. [51], who studied phosphate adsorption on γ-Al_2O_3 and kaolinite. Kaolinite (surrogate for mullite) showed a maximum adsorption capacity at near neutral pH, decreasing at low pH most likely due to the known dissolution of kaolinite under acidic conditions that results in the formation of $Al(OH)_3$ [51]. Reduced or stabilized phosphate sorption at low pH is attributed to the aqueous speciation of phosphate as a function of pH. At low levels of pH (< 2.1) the predominant dissolved phosphate species is H_3PO_4, which has less affinity for positively charged solids than $H_2PO_4^-$, HPO_4^{2-} and PO_4^{3-}. Recall that $H_2PO_4^-$ and HPO_4^{2-} are the predominant aqueous species for the pH range of 5 to 9 [13].

The total adsorption of phosphate in the fly ash surfaces at pH 4 was approximately 19%, much lower than the expected values based on the batch experiments. It is interesting; however, to notice that the adsorption of phosphate on kaolinite is negligible compared to hematite though some previous studies argued about the importance of mullite as an anion sorbing phase [45]. Our CCM predictions of phosphate immobilization are substantially less than the equilibration study and those results predicted by Goldberg et al. [24–26,28]. This is explained on the basis of the heterogeneity of the fly ash in comparison to the mineralogical purity of the natural and synthetic systems they

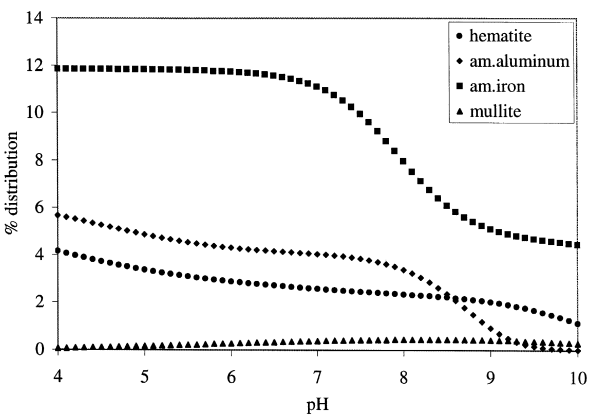

Fig. 6. Phosphorus adsorption (% distribution) on mineral phases modeled using the constant capacitance model (CCM).

studied and the fact that the constants determined for those media were far more representative of the total sample. While the approach of McCarthy et al. [39] was used, it is not known to what extent the adsorption parameters and site constants taken from pure geologic media are appropriate modeling acidic fly ash interactions with phosphate.

Nevertheless, for the amorphous and crystalline phases studied, the immobilization of phosphate in the Type F fly ash is attributed to the formation of insoluble aluminum and iron phosphates at low to medium values of pH. The crystalline phases played a minor role in phosphate immobilization. Therefore, it is concluded that the remaining 80% phosphate was immobilized by the amorphous phases of the type F fly ash and/or any precipitation reactions involving the amorphous phase such as those reported Veith and Sposito [46] between phosphate and allophanes (amorphous aluminosilicates), which are typically of volcanic origin and are characterized by a hollow spherules [52].

9. Conclusion

Batch equilibration experiments using a low calcium (~1 wt.% as CaO), acidic (pH ~ 4.5) Type F fly ash demonstrated phosphate immobilization on the order of 100% to 75% for 50 and 100 mg P/l solutions, respectively. A loosely compacted column of fly ash similarly removed 10 mg P/l for over 85 pore volumes. While the interactions between phosphate and calcium-rich (Type C) ashes are relatively well understood, insight into the mechanisms of phosphate immobilization in Type F ash necessitated a review of the phosphate chemistry and interactions with acidic geomedia. Phosphate adsorption was subsequently modeled using a constant capacitance approach (CCM) excluding precipitation reactions. Our CCM predictions of total phosphate immobilization (20%) were substantially less than the results of the batch equilibration experiments and phosphate adsorption predicted by other researchers examining near pure natural and synthetic geomedia due to the compositional heterogeneity of the fly ash. Nevertheless, for the amorphous and crystalline phases studied, the immobilization of phosphate in the Type F fly ash is attributed to the formation of insoluble aluminum and iron phosphates at low to medium values of pH.

Given the high removal of the phosphate and the fact that the authors could not locate studies focusing on the phosphate interactions with the amorphous phases of low calcium fly ashes, these interactions should be more fully evaluated. If these interactions can be quantified and predicted in high quality Type F ashes (low toxic metals), some interesting beneficiation opportunities may emerge for the ashes.

Acknowledgements

This effort was jointly supported by a National Science Foundation (NSF) Early Faculty CAREER Award (CMS-9703367) and funding and materials provided by Pennsylvania Power & Light (PP&L). The authors would like to express their gratitude to Messrs. Lawrence L. Labuz and Joel C. Pattishall (Ash Managers, PP&L) for their help and cooperation. Dr. Lisa Detter-Hoskin and Mr. Gautam Patel of the Georgia Tech

Research Institute are thanked for their assistance with the XRD and SEM analyses and interpretation of the results. Micromeretics (Norcross, GA) and Resource Materials Testing (Clermont, GA), respectively, completed the surface area measurements and XRF analyses on the fly ash. Part of the analyses conducted during the preparation of this paper were under the auspices of the course EAS8153: Mineral Surface Geochemistry taught by Dr. Patricia M. Dove of the School of Earth and Atmospheric Sciences at Georgia Tech. Mr. Michael C. Dodd performed the particle size analyses on the fly ash. Any opinions, findings, and conclusions expressed in this publication are those of the authors and do not necessarily reflect the views of NSF or PP&L.

References

[1] American Coal Ash Association (ACAA), 1997 — Combustion Products (CCP)Production and Use, Alexandria, VA,1998. http://www.acaa-usa.org/whatsnew/ccpcharts.htm.
[2] Metcalf & Eddy, Wastewater Engineering: Treatment/Disposal/Reuse, 2nd edn., McGraw-Hill, 1979, 920 pp.
[3] V.L. Snoeyink, D. Jenkins, Water Chemistry, Wiley, NY, 1980, p. 463.
[4] I. Kuziemska, Application of water extracted of brown coal fly ash to phosphate precipitation form polluted waters, Water Res. 14 (9) (1980) 1289–1293.
[5] L. Vordonis, P.G. Koutsoukos, A. Tzannini, A. Lycourghiotis, Uptake of inorganic orthophosphate by Greek fly ashes characterized using various techniques, Colloids Surf. 34 (1988) 55–68.
[6] A. Ugurlu, B. Salman, Phosphorous removal by fly ash, Environ. Int. 24 (8) (1998) 911–918.
[7] W.L. Stout, A.N. Sharpley, H.B. Pionke, Reducing phosphorous solubility with coal combustion by-products, J. Environ. Qual. 27 (1997) 111–118.
[8] T.L. Theis, J.L. Wirth, Sorptive behavior of trace metals on fly ash in aqueous systems, Environ. Sci . Technol. 11 (12) (1977) 1096–1100.
[9] Electrical Power Research Institute (EPRI), Land application of coal combustion by-products: use in agriculture and land reclamation, EPRI TR-103298, Research project 3207-01, Palo Alto, CA, 1995.
[10] B.P.J. Higgins, S.C. Mohleji, R.L. Irvine, Lake treatment with fly ash, lime and gypsum, J. WPCF 48 (9) (1976) 2153–2164, September.
[11] L.O. Fine, W.P. Jensen, Phosphate in waters: I. Reduction using Northern lignite fly ash, Water Resour. Bull. 17 (5) (1981) 895–897, October.
[12] Z. Amjad, P.G. Koutsoukos, G.H. Nancollas, The crystallization of hydroxyapatite and fluorapatite in the presence of magnesium ions, J. C.I.S. 101 (1) (1984) 250–256.
[13] W. Stumm, J.J. Morgan, Aquatic Chemistry, 3rd edn., Wiley, NY, 1996, 780 pp.
[14] D. Jenkins, J.F. Ferguson, A.B. Menar, Chemical processes for phosphate removal, Water Res. 5 (1971) 369–389.
[15] R.D. Neufeld, G. Thodos, Removal of orthophosphate form aqueous solution with activated alumina, Environ. Sci. Technol. 3 (7) (1969) 661–667.
[16] P.C. Singer, Anaerobic control of phosphate by ferrous iron, J. WPCF 44 (4) (1972) 663–669.
[17] S.J. Shiao, K. Akashi, Phosphate removal from aqueous solution from activated red mud, J. WPCF (1977) 280–285, February.
[18] H. Yamada, M. Kayama, K. Saito, M. Hara, A fundamental research on phosphate removal by using slag, Water Res. 20 (5) (1986) 547–557.
[19] M. Edwards, B. Courtney, P.S. Heppler, M. Hernandez, Beneficial discharge of iron coagulation sludge to sewers, J. Environ. Eng. 123 (10) (1997) 1027–1032.
[20] M.J. Baker, D.W. Blowes, C.J. Ptacek, Laboratory development of permeable reactive mixtures for the removal of phosphorous form onsite wastewater disposal systems, Environ. Sci. Technol. 32 (15) (1998) 2308–2316.

[21] A. Wild, The retention of phosphate by soil. A review, J. Soil Sci. 1 (2) (1950) 221–238.
[22] R.L. Parfitt, J.D. Russell, Adsorption on hydrous oxides: IV. Mechanisms of adsorption of various ions on goethite, J. Soil Sci. 28 (1977) 297–305.
[23] R.E. White, A.W. Taylor, Effect of pH on phosphate adsorption and isotopic exchange in acid soils at low and high additions of soluble phosphate, J. Soil Sci. 28 (1977) 48–61.
[24] S. Goldberg, G. Sposito, A chemical model of phosphate adsorption by soils: I. Reference oxide minerals, Soil Sci. Soc. Am. J. 48 (1984) 772–778.
[25] S. Goldberg, G. Sposito, A chemical model of phosphate adsorption by soils: II. Non-calcareous soils, Soil Sci. Soc. Am. J. 48 (1984) 779–783.
[26] S. Goldberg, Chemical modeling of anion competition on goethite using the constant capacitance model, Soil Sci. Soc. Am. J. 49 (1985) 851–856.
[27] N.J. Barrow, A.S. Ellis, Testing a mechanistic model: V. The points of zero effect for phosphate retention, for zinc retention and for acid/alkali titration of a soil, J. Soil Sci. 37 (1986) 303–310.
[28] S. Goldberg, S.J. Traina, Chemical modeling of anion competition on oxides using constant capacitance model-mixed-ligand approach, Soil Sci. Soc. Am. J. 51 (1987) 929–932.
[29] R.R. Martin, R. Smart, X-ray photoelectron studies of anion adsorption on goethite, Soil Sci. Soc. Am. J. 51 (1987) 54–56.
[30] R.R. Martin, R. Smart, K. Tazaki, Direct observation of phosphate precipitation in the goethite/phosphate system, Soil Sci. Soc. Am. J. 52 (1988) 1492–1500.
[31] V. Barron, M. Herruzo, J. Torrent, Phosphate adsorption by aluminous hematites of different shapes, Soil Sci. Soc. Am. J. 52 (1988) 647–651.
[32] J. Torrent, U. Schwertmann, V. Barrón, Fast and slow phosphate adsorption by goethite-rich natural materials, Clays Clay Miner. 40 (1) (1992) 14–21.
[33] J. Torrent, V. Barrón, U. Schwertmann, Phosphate adsorption and desorption by goethite differing in crystal morphology, Soil Sci. Soc. Am. J. 54 (1990) 1007–1012.
[34] R.L. Parfitt, R.J. Atkinson, R. Smart, The mechanism of phosphate fixation by iron oxides, Soil Sci. Soc. Am. 39 (1975) 837–841.
[35] J.T. Sims, B.G. Ellis, Changes in phosphorous adsorption associated with aging of aluminum hydroxide suspensions, Soil Sci. Soc. Am. J. 47 (1987) 912–916.
[36] M.J. Dudas, C.J. Warren, Submicroscopic structure and characteristics of intermediate-calcium fly ashes, Mater. Res. Soc. Symp. Proc. 113 (1988) 309–316.
[37] G.J. McCarthy, J.K. Solem, O.E. Manz, D.J. Hassett, Use of a database of chemical, mineralogical and physical properties of North American fly ash to study the nature of fly ash and its utilization as a mineral admixture in concrete, Mater. Res. Soc. Symp. Proc. 178 (1990) 3–33.
[38] R.T. Hemmings, E.E. Berry, On the glass in coal fly ashes: recent advances, Mater. Res. Soc. Symp. Proc. 113 (1988) 3–38.
[39] G.J. McCarthy, X-ray powder diffraction for studying the mineralogy of fly ash, Mater. Res. Soc. Symp. Proc. 113 (1988) 75–86.
[40] G.J. De Groot, J. Wijkstra, D. Hoede, H.A. van der Sloot, Leaching characteristics of selected elements from coal fly ash as a function of acidity of the contact solution and the liquid/solid ratio, in: P.L. Coté, T.M. Gilliam (Eds.), Environmental Aspects of Stabilization and Solidification of Hazardous and Radioactive Wastes, ASTM STP 1033, Philadelphia, PA, 1989, pp. 170–183.
[41] R.H. Yoon, T. Salman, G. Donnay, Predicting points of zero charge of oxides and hydroxides, J. C.I.S. 70 (3) (1979) 483–493.
[42] G. Sposito, The Surface Chemistry of Soils, Oxford Univ. Press, NY, 1984, 234 pp.
[43] J.A. Davies, D.B. Kent, Surface complexation modeling in aqueous geochemistry, Mineral–Water Interface Geochemistry, Reviews in Mineralogy vol. 23, 1990, pp. 177–260, Chapter 5.
[44] A. Breeuswama, J. Lyklema, Physical and chemical adsorption of ions in the electrical double layer on hematite (α-Fe_2O_3), J. C.I.S. 43 (1973) 437–448.
[45] E.E. van der Hoek, P.A. Bonouvrie, R.N.J. Comans, Sorption of As and Se on mineral components of fly ash: relevance for leaching processes, Appl. Geochem. 9 (1994) 403–412.
[46] J.A. Veith, G. Sposito, Reactions of aluminosilicates, aluminum hydrous oxides, and aluminum oxides with *o*-phosphate: the formation of X-ray amorphous analogs to of variscite and montebarisite, Soil Sci. Soc. Am. J. 41 (1977) 870–876.

[47] T.L. Yuan, Adsorption of phosphate and water-extractable soil organic material by synthetic aluminum silicates and acid soils, Soil Sci. Soc. Am. J. 44 (1980) 951–955.
[48] C. Papelis, K. Hayes, J. Leckie, HYDRAQL Manual, Department of Civil Engineering, Stanford University, Stanford, CA, 1988, 130 pp.
[49] S. Goldberg, R.A. Glaubig, Anion sorption on a calcareous, montmorillonitic soil-selenium, Soil Sci. Soc. Am. J. 52 (1988) 954–958.
[50] S. Goldberg, R.A. Glaubig, Anion sorption on a calcareous, montmorillonitic soil-arsenic, Soil Sci. Soc. Am. J. 52 (1988) 1297–1300.
[51] L.M. He, L.W. Zelazny, V.C. Baligar, K.D. Ritchey, D.C. Martens, Ionic strength effects on sulfate and phosphate adsorption on γ-alumina and kaolinite: triple layer model, Soil Sci. Soc. Am. J. 61 (1997) 784–793.
[52] K. Wada, Allophane and imogolite, Minerals in Soil Environments, Soil Science Society of America, Madison, WI, 1986, pp. 603–638, Chapter 16.
[53] M.A. Anderson, D.T. Malotky, The adsorption of protolyzable anions on hydrous oxides at the isoelectric pH, Journal of Colloid and Interface Science 72 (1979) 413–427.
[54] S.S.S. Rajan, K.W. Perrott, W.M.H. Saunders, Identification of phosphate-reactive sites of hydrous alumina from proton consumption during phosphate adsorption at constant pH values, Journal of Soil Science 25 (1974) 438–447.
[55] C.P. Huang, W. Stumm, Specific adsorption of cations on hydrous γ-Al_2O_3, Journal of Colloid and Interface Science 43 (1973) 409–420.